PHYSICAL REVIEW D **75,** 023512 (2007)

Power-law parametrized quintessence model

Sohrab Rahvar[1] and M. Sadegh Movahed[1,2]

[1]*Department of Physics, Sharif University of Technology, P.O. Box 11365-9161, Tehran, Iran*
[2]*Institute for Studies in Theoretical Physics and Mathematics, P.O. Box 19395-5531, Tehran, Iran*

(Received 3 August 2006; published 11 January 2007)

We propose a simple power-law parametrized quintessence model with time-varying equation of state and obtain corresponding quintessence potential of this model. This model is compared with Supernova Type Ia (SNIa) Gold sample data, size of baryonic acoustic peak from Sloan Digital Sky Survey (SDSS), the position of the acoustic peak from the CMB observations and structure formation from the 2dFGRS survey and put constrain on the parameters of model. The parameters from the best fit indicates that the equation of state of this model at the present time is $w_0 = -1.40^{+0.40}_{-0.65}$ at 1σ confidence level. Finally we calculate the age of universe in this model and compare it with the age of old cosmological objects.

DOI: 10.1103/PhysRevD.75.023512 PACS numbers: 98.80.Es, 95.36.+x, 98.62.Py

I. INTRODUCTION

Observations of the apparent magnitude and redshift of type Ia supernovas (SNIa) provide the main evidence for the positive acceleration of the Universe [1,2]. A combined analysis of SNIa data and the cosmic microwave background radiation (CMB) indicates that the dark energy filled about $2/3$ of the total energy of the Universe and the remained part is dark matter with a few percent in the form of baryonic matter [3–5].

The ''cosmological constant'' is a possible explaining for the acceleration of the universe [6]. This geometrical term at the right hand side of the Einstein field equation can be regarded as a fluid with the equation of state of $w = -1$. However, there are two problems with the cosmological constant, namely, the *fine-tuning* and the *cosmic coincidence*. In the framework of quantum field theory, the vacuum expected value is 123 order of magnitude larger that the observed value of 10^{-47} GeV^4. The absence of a fundamental mechanism which sets the cosmological constant zero or very small value is the cosmological constant problem. The second problem as the cosmic coincidence, states that why are the energy densities of dark energy and dark matter nearly equal today? In another word, to fulfill the present condition, cosmological constant has to be fine tuned at very early universe.

One of the solutions to this problem is a model with varying cosmological constant decays from the beginning of the universe to a small value at the present time. A nondissipative minimally coupled scalar field, so-called quintessence model can play the role of time-varying cosmological constant [7–9]. The ratio of energy density of this field to the matter density increases by the expansion of the universe and after a while the dark energy becomes the dominant energy in the universe. One of the features of the quintessence models is the variation of the equation of state of dark energy during the expansion of the universe. Various quintessence models as k-essence [10], tachyonic matter [11], Phantom [12,13] and Chaplygin gas [14] provide various equation of states for the dark energy [13,15–22].

There are also phenomenological models as the parametrization of the equation of state of dark energy in terms of redshift [23–25]. For a dark energy with the equation of state of $p_X = w\rho_X$, using the continuity equation, the density of dark energy changes with the scale factor as

$$\rho_X = \rho_X^{(0)} a^{-3(1+\bar{w}(a))}, \tag{1}$$

where $\bar{w}(a)$ is the mean of the equation of state in the logarithmic scale

$$\bar{w}(a) = \frac{\int_1^a w(a')d\ln(a')}{\int_1^a d\ln(a')}. \tag{2}$$

The main aim of the phenomenological models is to remove the fine-tuning of dark energy by means that the ratio of dark energy density to the matter ($\rho_m \sim a^{-3}$),

$$\frac{\rho_X}{\rho_m} = \frac{\rho_X^{(0)}}{\rho_m^{(0)}} a^{-3\bar{w}(a)} \tag{3}$$

approach to unity at the early universe in contrast to a very small value in the case of cosmological constant. Here we propose a simple power-law model for the mean value of equation of state as

$$\bar{w}(a) = w_0 a^\alpha, \tag{4}$$

This model is expressed with the two parameter of w_0 (equation of state at the present time) and the exponent of α. The radio of dark energy to the matter in terms of the scale factor is plotted in Fig. 1, shows that the dark energy and matter densities at the early universe are in the same order. The equation of state of this model according to the definition of $\bar{w}(a)$ obtain as

$$w(a) = w_0 a^\alpha (1 + \ln a^\alpha). \tag{5}$$

One of the features of this model is that for the scale factors in the range of $a < e^{-1/\alpha}$, the sign of the equation of state will change to the positive value. From Fig. 1 for $\alpha < 1.3$

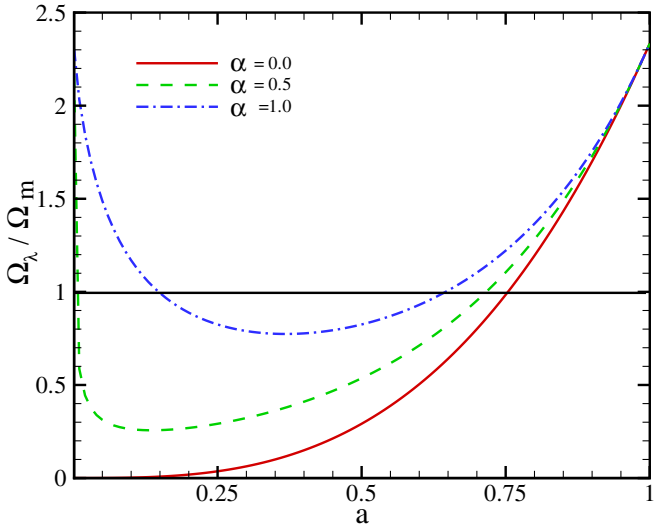

FIG. 1 (color online). Ratio of dark energy to the matter density as a function of scale factor. For $0 < \alpha < 1.3$ we have 2 times of dark energy dominance over the (cold dark) matter. We chose $w_0 = -1$, $\Omega_m = 0.3$ and $\Omega_{\rm tot} = 1.0$.

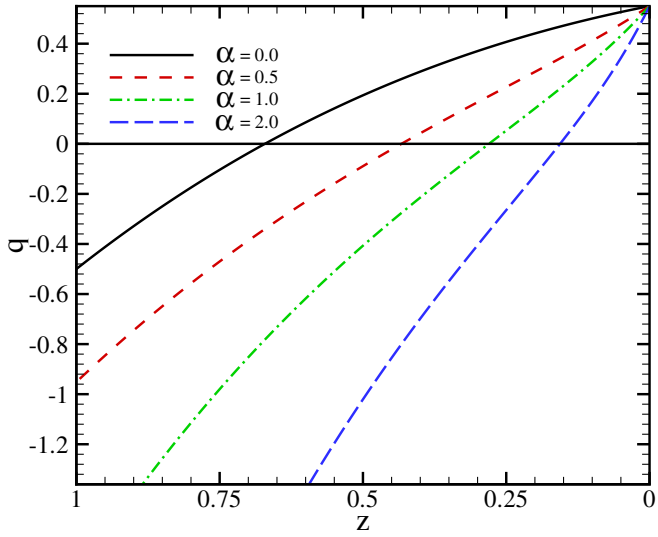

FIG. 2 (color online). Acceleration parameter ($q = \ddot{a}/H_0^2 a$) in the power-law model as a function of redshift for various values of α-exponent. Increasing α causes that universe to enter the acceleration phase at later times. We chose $w_0 = -1$, $\Omega_m = 0.3$ and $\Omega_{\rm tot} = 1.0$.

we have 2 times of domination of dark energy during the history of universe: once for the early universe and later at the lower redshifts. However, since the sign of the equation of state of dark energy at the early universe is positive, it will not accelerate the universe and we will have only a late time acceleration. One of the advantages of this model is that the ratio of corresponding energy density of power-law quintessence model to the matter energy density at the early universe is not sensitive to the choice of parameters of model. For the early universe as the scale factor goes to zero, we find that $\lim_{a\to 0}\Omega_\Lambda/\Omega_m = \Omega_\lambda/\Omega_m(a = 1)$ and this means that the dark energy density does not need to be fine tuned at $t \to 0$.

Figure 2 shows the acceleration parameter ($q = \ddot{a}/H_0^2 a$) of the universe in this model in terms of the scale factor for various values of α. Increasing the α-exponent causes the universe to enter the acceleration phase at the later times but speed-up to enter the de Sitter phase faster (see Fig. 2).

The organization of the paper is as follows: In Sec. II we reconstruct a quintessence potential equivalent with the power-law parametrized model. In Sec. III we study the effect of this model on the age of Universe, comoving distance, comoving volume element and the variation of angular size by the redshift [26]. In Sec. IV we put constrain on the parameters of the model by the background evolution, such comparing with the Gold sample of Supernova Type Ia data [27], the position of the observed acoustic angular scale on CMB and the baryonic oscillation length scale. We study the linear structure formation in this model and compare the growth index with the observations from the 2-degree Field Galaxy Redshift Survey (2dFGRS) data in Sec. V. We also compare the age of the universe in this model with the age of old cosmological structures. Sec. VI contains summary and conclusion of this work.

II. CORRESPONDING QUINTESSENCE POTENTIAL OF POWER-LAW DARK ENERGY

One of the mechanism to generate a time-varying dark energy is using a scalar field that can provide a positive acceleration for the universe at the present time. The essential condition for a given scalar field to play the role of dark energy is that the equation of state at the lower redshifts can provide the condition of $w < -1/3$. From the Lagrangian of uniform scalar field with the potential term of $V(\phi)$ and kinetic term of $\dot{\phi}^2/2$, the energy density and pressure is as follows:

$$\rho_X = \tfrac{1}{2}\dot{\phi}^2 + V(\phi) \tag{6}$$

$$P_X = \tfrac{1}{2}\dot{\phi}^2 - V(\phi). \tag{7}$$

Using, the definition of equation of state of dark energy, $w = P_X/\rho_X$, the equation of state in terms of kinetic and potential energies of scalar field can be written as

$$w = \frac{T - V}{T + V}. \tag{8}$$

The kinetic and potential energies of scalar field from the Eqs. (7) and (8) in terms of ρ_X and the equation of state of dark energy obtain as

$$T = \tfrac{1}{2}\rho_X(1 + w) \tag{9}$$

$$V = \tfrac{1}{2}\rho_X(1 - w). \tag{10}$$

For a positive T and V the equation of state is bounded to the interval $-1 < w < +1$. For $T > 0$ and $V < 0$ we have $|w| > 1$ and for the case of $T < 0$ the equation of state can be $w < -1$ (i.e. kinetic term of Lagrangian has negative sign). Here we reconstruct a scalar potential which can generate the power-law quintessence model. The kinetic term of the scalar potential from the Eq. (9) in terms of redshift obtain as

$$\frac{d\phi}{dz} = \pm \frac{[\rho_X(z)(1+w)]^{1/2}}{H(z)(1+z)}, \tag{11}$$

where the minus or plus sign are chosen if $\dot{\phi} > 0$ and $\dot{\phi} < 0$, respectively. Choosing the sign is arbitrary as it can be changed by the field redefinition of $\phi \rightarrow -\phi$. Here we choose the negative sign for convenient. The Hubble parameter also is given by

$$H^2(z; \alpha, w_0, \Omega_m) = H_0^2[\Omega_m(1+z)^3 + (1-\Omega_m)(1+z)^{3[1+\bar{w}(z;\alpha,w_0)]}]. \tag{12}$$

We substitute the Hubble parameter in Eq. (11) and for the Hubble parameter at the present time we replace with $H_0^2 = \rho_c^{(0)}/3M_{\rm pl}^2$, where $\rho_c^{(0)}$ is the critical density at the present time and $M_{\rm pl}$ is the Planck mass. From the numerical integration of Eq. (11) we obtain the dependence of the scalar field, $\tilde{\phi} = \phi/M_{\rm pl}$ in terms of the redshift (see Fig. 3). On the other hand from the Eq. (10) we can obtain the quintessence potential in terms of redshift

$$\tilde{V}(z) = \tfrac{1}{2}(1-w)F(z), \tag{13}$$

where $F(z) = \rho_X(z)/\rho_X(0)$ and $\tilde{V}(z) = V(z)/V(0)$. We eliminate numerically the redshift between the scalar field, $\tilde{\phi} = \tilde{\phi}(z)$ and potential in Eq. (13) and obtain an explicit relation between the potential and scalar field as shown in Fig. 4. The shape of potential shows the scalar field starts to role from $\tilde{\phi} \sim 0$ at high redshifts, and at the low redshifts we have a slow role condition, similar to the inflationary scenarios. The dependence of the kinetic term of the scalar filed in terms of the scale factor for various equation of state at the present time (w_0) is shown in Fig. 5. For the case of $w_0 < -1$, we will have negative kinetic term at the present time.

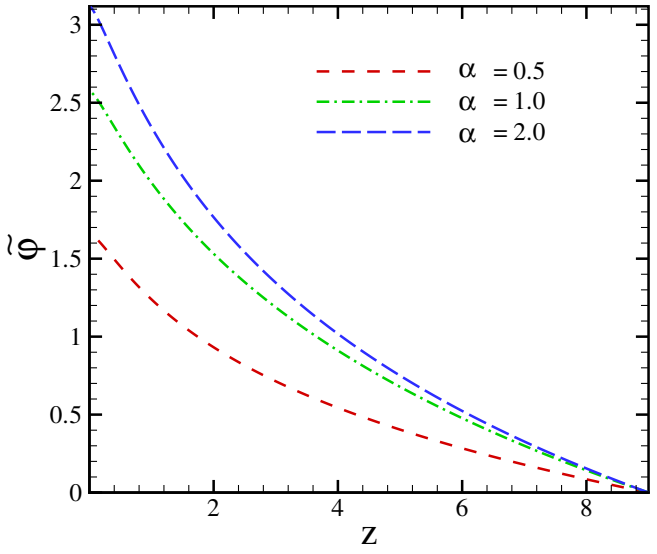

FIG. 3 (color online). Dependence of scalar field $\tilde{\phi} = \tilde{\phi}(z)$ to the redshift in power-law dark energy model. The curve results from the numerical solution of Eq. (11).

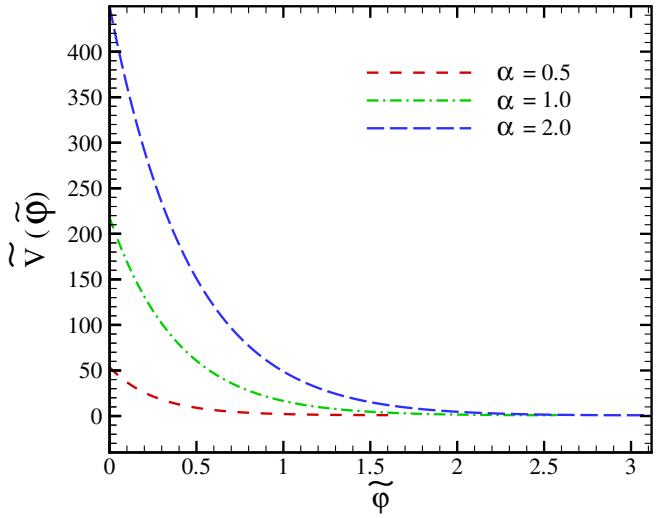

FIG. 4 (color online). Dependence of exponential potential to the scale factor in power-law quintessence model.

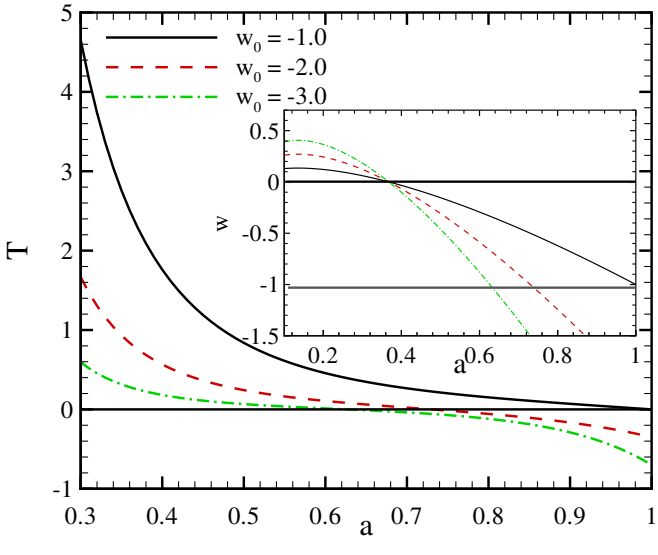

FIG. 5 (color online). Kinetic term in terms of scale factor for various equetion of state at the present time. The equation of state as a function of scale factor also represented in the smaller figure. Here we chose $\Omega_m = 0.30$ and $\alpha = 1.0$.

III. THE EFFECT OF VARIABLE DARK ENERGY ON THE GEOMETRICAL PARAMETERS OF UNIVERSE

The cosmological observations are mainly affected by the background dynamics of universe. In this section we study the effect of the power-law dark energy model on the geometrical parameters of universe.

A. Comoving distance

The radial comoving distance is one of the basis parameters in cosmology. For an object with the redshift of z, using the null geodesics in the FRW metric, the comoving distance obtain as

$$r(z;\alpha, w_0, \Omega_m) = \int_0^z \frac{dz'}{H(z';\alpha, w_0, \Omega_m)}, \qquad (14)$$

where $H(z;\alpha, w_0, \Omega_m)$ is the Hubble parameter and we can express it in terms H_0 and matter and dark energy density of the universe at the present time.

By numerical integration of Eq. (14), the comoving distance in terms of redshift for the case of $w_0 = -1$ and $\Omega_m = 0.3$ for different values of α is shown in Fig. 6. Increasing the α exponent, leads the dark energy dominant at the higher redshifts and results a smaller comoving distance. One of the main applications of the comoving distance calculation is on analyzing of the luminosity distance of SNIa data.

B. Angular size

Measurement of apparent angular size of an object located at the cosmological distance is another important parameter that can be affected by the amount and variation of dark energy during the history of universe. Distance between two points in the flat universe with the comoving size of D, located at the comoving distance of r from the observed is seen with the angular separation of

$$\theta = \frac{D}{r}. \qquad (15)$$

Here we assume that the distance between two points increases with the expansion of the universe. The main applications of Eq. (15) is on the measurement of the apparent angular size of acoustic peak on CMB and baryonic acoustic peak at the lower redshifts. By measuring the angular size in different redshifts (so-called Alcock-Paczynski test) it is possible to probe the variability of dark energy [26]. The variation of apparent angular size $\Delta\theta$ in terms Δz from Eq. (15) is given by

$$\frac{\Delta z}{\Delta\theta} = \frac{H(z;\alpha, w_0, \Omega_m) r(z;\alpha, w_0, \Omega_m)}{\theta}. \qquad (16)$$

Figure 7 shows $\Delta z/\Delta\theta$ in terms of redshift, normalized to the case with $\alpha = 0$ and $w_0 = -1$ (i.e. ΛCDM model). The advantage of Alcock-Paczynski test is that it is independent of standard candles and a standard ruler such as the size of baryonic acoustic peak can be used to constrain the dark energy model.

C. Comoving volume element

The comoving volume element is an other geometrical parameter which is used in number-count tests such as lensed quasars, galaxies, or clusters of galaxies. The comoving volume element in terms of comoving distance and Hubble parameters is given by

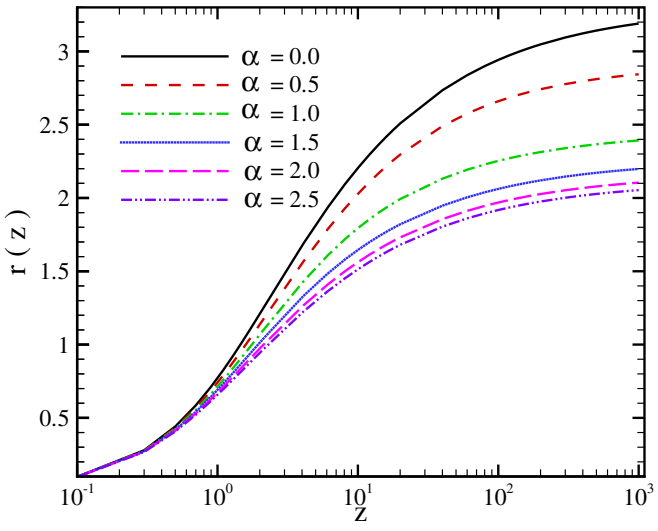

FIG. 6 (color online). Comoving distance, $r(z;\alpha, w_0, \Omega_m)$ (in unit of c/H_0) as a function of redshift for various values of α. We chose $w_0 = -1$, $\Omega_m = 0.3$ and $\Omega_{\rm tot} = 1.0$.

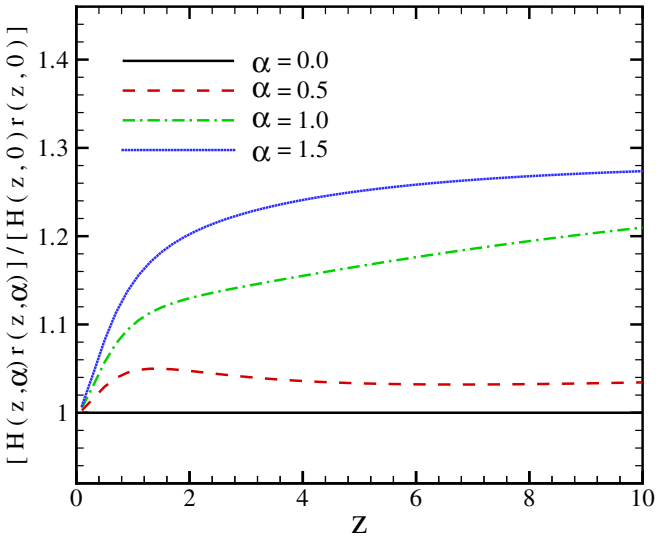

FIG. 7 (color online). Alcock-Paczynski test, compares $\Delta z/\Delta\theta$ normalized to the case of ΛCDM model as a function of redshift for four different αs. We chose $w_0 = -1$, $\Omega_m = 0.3$ and $\Omega_{\rm tot} = 1.0$.

$$f(z;\alpha,w_0,\Omega_m) \equiv \frac{dV}{dzd\Omega} = r^2(z;\alpha,w_0,\Omega_m)/H(z;\alpha,w_0,\Omega_m). \quad (17)$$

According to Fig. 8, the comoving volume element becomes maximum around $z \simeq 2$. For a larger α exponents, the position of the peak in the comoving volume element shifts to the lower redshifts.

D. Age of universe

The "age crisis" is one the main reasons for the existence of dark energy. The problem is that the universe's age in the cold dark matter (CDM) universe is less than the age of old stars in it. Studies on the old stars [28] suggests an age of 13^{+4}_{-2} Gyr for the universe. Richer *et al.* [29] and Hasen *et al.* [30] also proposed an age of 12.7 ± 0.7 Gyr, using the white dwarf cooling sequence method (for full review of the cosmic age see [5]). The age of universe integrating from the big bang up until now can be obtained as

$$t_0(\alpha,w_0,\Omega_m) = \int_0^{t_0} dt = \int_0^{\infty} \frac{dz}{(1+z)H(z;\alpha,w_0,\Omega_m)}, \quad (18)$$

Figure 9 shows the dependence of H_0t_0 (Hubble parameters times the age of universe) in terms of α-exponent for a typical values of cosmological parameters (e.g. $\Omega_m = 0.3$ and $w_0 = -1$ in flat universe). Increasing α results a shorter age for the universe.

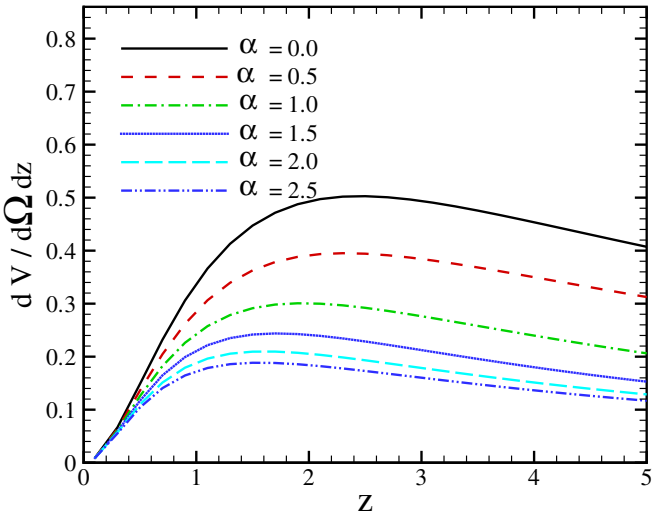

FIG. 8 (color online). The comoving volume element in terms of redshift for various α exponents. Increasing α shifts the position of maximum value of the volume element to the lower redshifts. We chose $w_0 = -1$, $\Omega_m = 0.3$ and $\Omega_{\rm tot} = 1.0$.

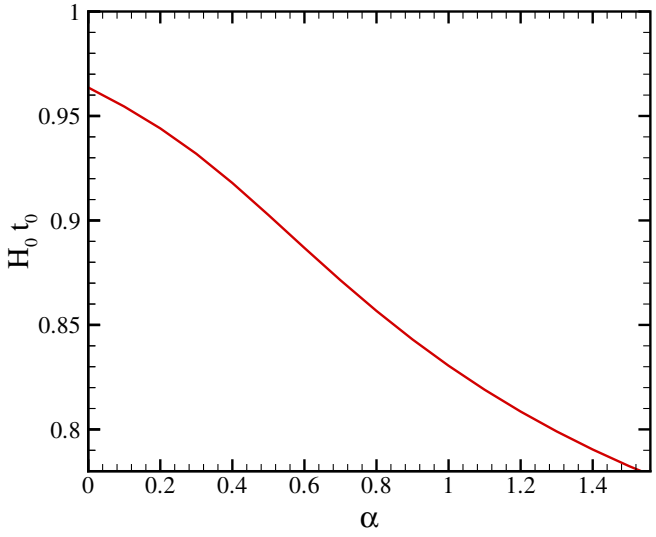

FIG. 9 (color online). H_0t_0 (age of universe times the Hubble constant at the present time) as a function of α. We choose the cosmological parameters in flat universe as $\Omega_m = 0.3$ and $w_0 = -1.0$ (H_0t_0 does not depend on h). Increasing α-exponent makes a shorter age for the universe.

IV. OBSERVATIONAL CONSTRAINT FROM THE BACKGROUND EVOLUTION

In this section we compare the SNIa Gold sample data, the location of baryonic acoustic peak from the SDSS and the location of acoustic peak from the CMB observation to constrain the parameters of the model.

A. Examining model by Supernova type Ia: Gold sample

The Supernova Type Ia experiments provided the main evidence of the existence of dark energy. Since 1995 two teams of the *High-Z Supernova Search* and the *Supernova Cosmology Project* have been discovered several type Ia supernovas at the high redshifts [18,31]. Recently Riess *et al.* (2004) announced the discovery of 16 type Ia supernovas with the Hubble Space Telescope. This new sample includes 6 of the 7 most distant ($z > 1.25$) type Ia supernovas. They determined the luminosity distance of these supernovas and with the previously reported algorithms, obtained a uniform 157 Gold sample of type Ia supernovas [27,32,33]. In this subsection we compare the predictions of the dark energy model with the SNIa Gold sample. The apparent magnitude of supernovas m includes the reddening, K correction is related to the (dimensionless) luminosity distance, D_L, of a an object at redshift z through

$$m = \mathcal{M} + 5\log D_L(z;\alpha,w_0,\Omega_m), \quad (19)$$

where for a spatially flat universe we have

$$D_L(z;\alpha,w_0,\Omega_m) = H_0(1+z)\int_0^z \frac{d\zeta}{H(\zeta;\alpha,w_0,\Omega_m)}. \quad (20)$$

Also

$$\mathcal{M} = M + 5\log\left(\frac{c/H_0}{1\ \mathrm{Mpc}}\right) + 25. \quad (21)$$

where M is the absolute magnitude. The distance modulus, μ, is defined as

$$\mu \equiv m - M$$
$$= 5\log D_L(z; \alpha, w_0, \Omega_m) + 5\log\left(\frac{c/H_0}{1\ \mathrm{Mpc}}\right) + 25, \quad (22)$$

To compare the theoretical results with the observational data, we compute the distance modulus, as given by Eq. (22). We compare the distance modulus in dark energy model with that from the observation through the least squares fitting

$$\chi^2 = \sum_i \frac{[\mu_{\mathrm{obs}}(z_i) - \mu_{\mathrm{th}}(z_i; \Omega_m, w_0, \alpha, h)]^2}{\sigma_i^2}, \quad (23)$$

where σ_i is the observational uncertainty in the distance modulus. To constrain the parameters of model, we use the likelihood analysis. Marginalizing over the nuisance parameter of h in a flat universe ($\Omega_{\mathrm{tot}} = 1$), the best fit values for the parameters of model obtain as $w_0 = -2.60^{+1.80}_{-2.00}$, $\Omega_m = 0.45^{+0.09}_{-0.45}$ and $\alpha = 1.00^{+1.00}_{-1.00}$ with $\chi^2_{\mathrm{min}}/N_{\mathrm{d.o.f}} = 1.13$ at 1σ level of confidence. Priors on the parameter space in the likelihood analysis is given in Table I. We keep these priors in all the observational tests in the next section. The corresponding value for the Hubble parameter at the minimized χ^2 is $h = 0.66$ and since we have already marginalized over this parameter we do not assign an error bar for it. Figure 10 shows the best fit of model to the Gold sample of SNIa. We compare our result with that of Riess *et al.* (2004), for $\alpha = 0$ and recover their results (see Fig. 11).

For the age-consistency test we substitute the parameters of model from the SNIa fitting in Eq. (18) and obtain the age of universe about 13.19 Gry, which is in good agreement with the age of old stars.

B. Combined analysis: SNIa + CMB + SDSS

In this section we combine SNIa Gold sample, CMB data from the WMAP with recently observed baryonic peak from the SDSS to constrain the parameters of power-law dark energy model [37].

The angular size of the acoustic peak is the most relevant parameter in the spectrum of CMB which can be used to determine the geometry and the matter content of the universe. The acoustic peak corresponds to the Jeans length of photon-baryon structures at the last scattering surface

TABLE I. Priors on the parameter space, used in the likelihood analysis.

Parameter	Prior	
$\Omega_{\mathrm{tot}} = \Omega_m + \Omega_\lambda$	1.00	Fixed
Ω_m	$0.00 - 1.00$	Top hat
$\Omega_b h^2$	0.020 ± 0.005	Top hat (BBN)[34]
h	—	Free [35,36]
w_0	$-10.00 - 0.00$	Top hat
α	—	Free

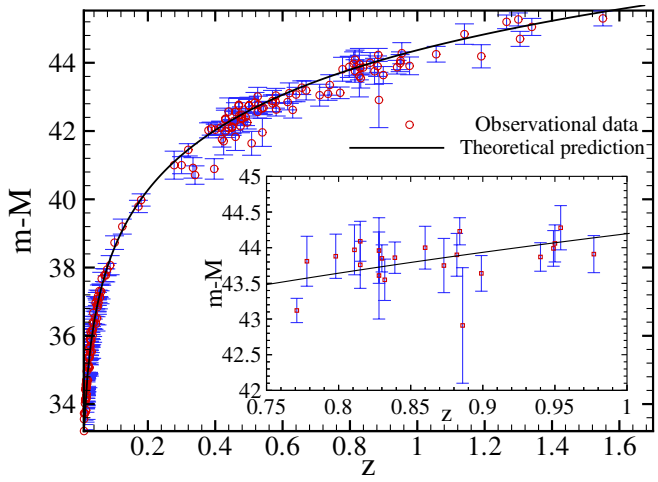

FIG. 10 (color online). Fitting the distance modulus of the SNIa Gold sample in terms of redshift with the power-law dark energy model. Solid-line shows the best fit with the corresponding parameters of $h = 0.66$, $w_0 = -2.60^{+1.80}_{-2.00}$, $\Omega_m = 0.45^{+0.09}_{-0.45}$ and $\alpha = 1.00^{+1.00}_{-1.00}$ in 1σ level of confidence with $\chi^2_{\mathrm{min}}/N_{\mathrm{d.o.f}} = 1.13$.

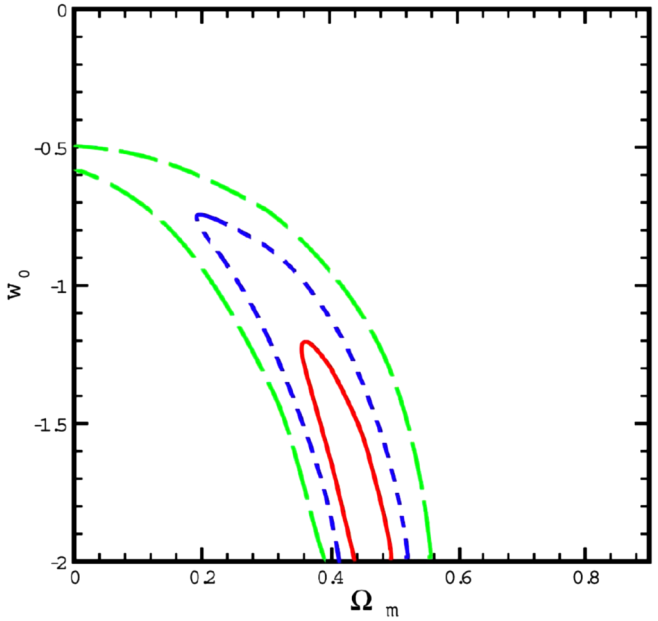

FIG. 11 (color online). Joint confidence intervals for Ω_m and w_0 for the case of $\alpha = 0$ with 1σ (solid line), 2σ (dashed line) and 3σ (long dashed line) confidence level. This result is in good agreement with that of Riess *et al.* (2004).

some ~379 Kyr after the big bang [5]. The apparent angular size of acoustic peak in a flat universe can be obtained by dividing the comoving size of sound horizon at the decoupling epoch $r_s(z_{\rm dec})$ to the comoving distance of observer to the last scattering surface $r(z_{\rm dec})$

$$\theta_A \equiv \frac{r_s(z_{\rm dec})}{r(z_{\rm dec})}. \tag{24}$$

The size of sound horizon at numerator of Eq. (24) corresponds to the distance that perturbation in pressure can travel from the beginning of universe up to the last scattering surface and is given by

$$r_s(z_{\rm dec}; \alpha, w_0, \Omega_m) = \int_{z_{\rm dec}}^{\infty} \frac{v_s(z)}{H(z; \alpha, w_0, \Omega_m)} dz, \tag{25}$$

where $v_s(z)^{-2} = 3 + 9/4 \times \rho_b(z)/\rho_r(z)$ is the sound velocity in the unit of speed of light from the big bang up to the last scattering surface, $\rho_b(z)$ and $\rho_r(z)$ are the energy density of baryonic and radiation, respectively [20,38].

Changing the parameters of the dark energy can change the size of apparent acoustic peak and subsequently the position of $l_A \equiv \pi/\theta_A$ in the power spectrum of temperature fluctuations on CMB. Here we plot the dependence of l_A on α and w_0 for a typical values of cosmological parameters (see Fig. 12). In order to compare the observed angular size of acoustic peak with the dark energy model, we use the shift parameter R as [39]

$$R = \sqrt{\Omega_m} \int_0^{z_{\rm dec}} \frac{dz}{E(z; \alpha, w_0, \Omega_m)}, \tag{26}$$

where $E(z; \alpha, w_0, \Omega_m) = H(z; \alpha, w_0, \Omega_m)/H_0$. The shift parameter is proportional to the size of acoustic peak to

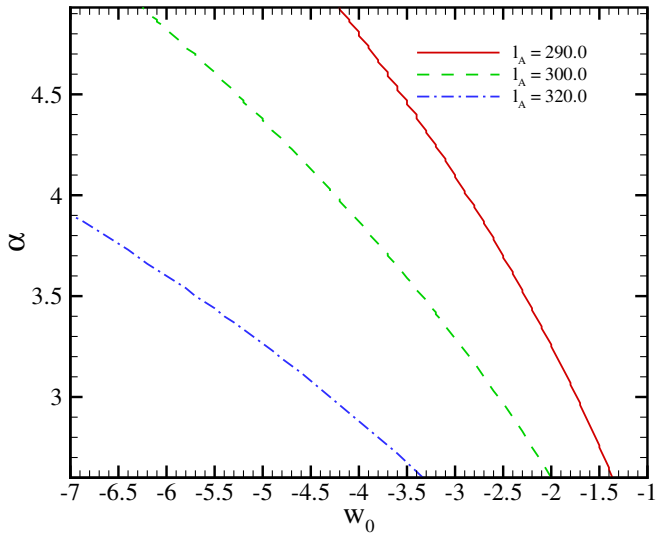

FIG. 12 (color online). Dependence of acoustic angular scale l_A on α and w_0 for the three cases of $l_A = 290$ (solid line), 300 (dashed line) and 320 (dashed-dotted line). We chose $\Omega_m = 0.3$ and $\Omega_{\rm tot} = 1.0$.

that of flat pure-CDM, $\Lambda = 0$ model, ($R \propto \theta_A/\theta_A^{\rm flat}$). The observational result of CMB experiments correspond a shift parameter of $R = 1.716 \pm 0.062$ (given by WMAP, CBI, ACBAR) [5,40]. One of the advantages of using the parameter R is that it is independent of Hubble constant.

Recently detected size of baryonic peak in the SDSS is the third observational data for our analysis. The correlation function of 46 748 *Luminous Red Galaxies* (LRG) from the SDSS shows a well detected baryonic peak around 100 Mpc h^{-1}. This peak has an excellent match to the predicted shape and the location of the imprint of the recombination-epoch acoustic oscillation on the low-redshift clustering matter [41]. For a flat universe we can construct the parameter A as follows:

$$A = \sqrt{\Omega_m} E(z_1; \alpha, w_0, \Omega_m)^{-1/3} \left[\frac{1}{z_1} \times \int_0^{z_1} \frac{dz}{E(z; \alpha, w_0, \Omega_m)} \right]^{2/3}. \tag{27}$$

We use the robust constraint on the dark energy model using the value of $A = 0.469 \pm 0.017$ from the LRG observation at $z_1 = 0.35$ [41].

In what follows we perform a combined analysis of SNIa, CMB and SDSS to constrain the parameters of dark energy model by minimizing the combined $\chi^2 = \chi^2_{\rm SNIa} + \chi^2_{\rm CMB} + \chi^2_{\rm SDSS}$. The best values of the model parameters from the fitting with the corresponding error bars from the likelihood function marginalizing over the Hubble parameter in the multidimensional parameter space results: $\Omega_m = 0.32^{+0.03}_{-0.04}$, $\alpha = 1.60^{+0.60}_{-0.90}$ and $w_0 = -2.00^{+0.80}_{-0.40}$ at 1σ confidence level with $\chi^2_{\rm min}/N_{\rm d.o.f} = 1.13$. The Hubble parameter corresponds to the minimum value of χ^2 is $h = 0.66$. Here we obtain an age of 12.82 Gyr for the universe. Table II indicates the best fit values for the cosmological parameters with one and two σ level of confidence.

TABLE II. The best values for the parameters of power-law dark energy model with the corresponding age for the universe from the fitting with the SNIa, SNIa + CMB + SDSS and SNIa + CMB + SDSS + LSS experiments at one and two σ confidence level.

Observation	Ω_m	α	w_0	age (Gyr)
SNIa	$0.45^{+0.09}_{-0.45}$	$1.00^{+1.00}_{-1.00}$	$-2.60^{+1.80}_{-2.00}$	13.19
	$0.45^{+0.13}_{-0.45}$	$1.00^{+2.00}_{-1.00}$	$-2.60^{+1.90}_{-2.90}$	
SNIa + CMB + SDSS	$0.32^{+0.03}_{-0.04}$	$1.60^{+0.60}_{-0.90}$	$-2.00^{+0.80}_{-0.40}$	12.82
	$0.32^{+0.05}_{-0.08}$	$1.60^{+1.40}_{-1.60}$	$-2.00^{+1.30}_{-1.30}$	
SNIa + CMB + SDSS + LSS	$0.31^{+0.02}_{-0.04}$	$0.80^{+0.70}_{-0.30}$	$-1.40^{+0.40}_{-0.65}$	13.72
	$0.31^{+0.04}_{-0.06}$	$0.80^{+1.60}_{-0.80}$	$-1.40^{+0.60}_{-1.10}$	

V. CONSTRAINTS BY LARGE SCALE STRUCTURE

So far we have only considered observations related to the background evolution. In this section using the linear approximation of structure formation we obtain the growth index of structures and compare it with result of observations by the 2-degree Field Galaxy Redshift Survey (2dFGRS).

The continuity and Poisson equations for the density contrast $\delta = \delta\rho/\bar{\rho}$ in the cosmic fluid provides the evolution of density contrast in the linear approximation (i.e. $\delta \ll 1$)[42,43] as

$$\ddot{\delta} + 2\frac{\dot{a}}{a}\dot{\delta} - (v_s{}^2\nabla^2 + 4\pi G\rho)\delta = 0, \tag{28}$$

where the dot denotes the derivative with respect to time. The effect of dark energy in the evolution of the structures in this equation enters through its influence on the expansion rate. Here we assume that dark energy distributed uniformly as the background fluid and does not contribute in clustering of matter. The validity of the linear Newtonian approach is restricted to perturbations on the subhorizon scales but large enough where structure formation is still in the linear regime [42,43]. For the perturbations larger than the Jeans length, $\lambda_J = \pi^{1/2}v_s/\sqrt{G\rho}$, Eq. (28) for CDM reduces to

$$\ddot{\delta} + 2\frac{\dot{a}}{a}\dot{\delta} - 4\pi G\rho\delta = 0. \tag{29}$$

The equation for the evolution of density contrast can be rewritten in terms of scale factor as

$$\frac{d^2\delta}{da^2} + \frac{d\delta}{da}\left[\frac{\ddot{a}}{\dot{a}^2} + \frac{2H}{\dot{a}}\right] - \frac{3H_0^2}{2\dot{a}^2a^3}\Omega_m\delta = 0, \tag{30}$$

where dot denotes the time derivative. Numerical solution of Eq. (30) in the FRW universe with the power-law dark energy model is shown in Fig. 13. In the CDM model, the density contrast δ grows linearly with the scale factor, while we have a deviation from the linearity as soon as dark energy begins to dominate. As larger α is, universe enters the dark energy domination earlier (see Fig. 1) which results in a lesser growth of the density contrast.

In the linear perturbation theory, the peculiar velocity field $\mathbf{v}$ is determined by the density contrast [42,44] as

$$\mathbf{v}(\mathbf{x}) = H_0\frac{f}{4\pi}\int \delta(\mathbf{y})\frac{\mathbf{x}-\mathbf{y}}{|\mathbf{x}-\mathbf{y}|^3}d^3\mathbf{y}, \tag{31}$$

where the growth index f is defined by

$$f = \frac{d\ln\delta}{d\ln a}, \tag{32}$$

and it is proportional to the ratio of the second term of Eq. (29) (friction) by the third (Poisson) term.

We use the evolution of the density contrast δ to compute the growth index of structure f, which is an important quantity for the interpretation of peculiar velocities of galaxies, as discussed in [44,45] for the Newtonian and the relativistic regime of structure formation. Replacing the density contrast with the growth index in Eq. (30) results in the evolution of growth index as

$$\frac{df}{d\ln a} = \frac{3H_0^2}{2\dot{a}^2a}\Omega_m - f^2 - f\left[2 - \frac{H_0^2}{2}\left[\frac{2}{H_0^2} + \frac{\Omega_m}{a^3} + \Omega_\Lambda(a)(1+3w(a))\right]\right]. \tag{33}$$

Figure 14 shows the numerical solution of (33) in terms of redshift.

The observation of 220 000 galaxies with the 2dFGRS experiment provides the numerical value of growth index [41]. By measurements of two-point correlation function, the 2dFGRS team reported the redshift distortion parame-

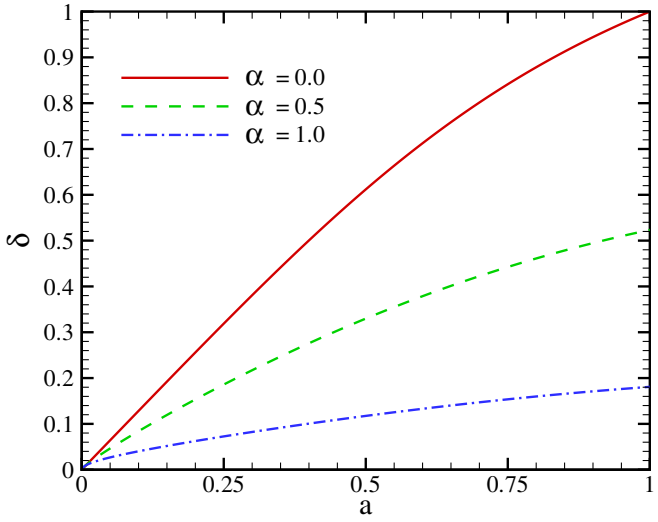

FIG. 13 (color online). Evolution of density contrast as a function of scale factor for different values of α exponent in the flat universe with $\Omega_m = 0.3$ and $w_0 = -1.0$.

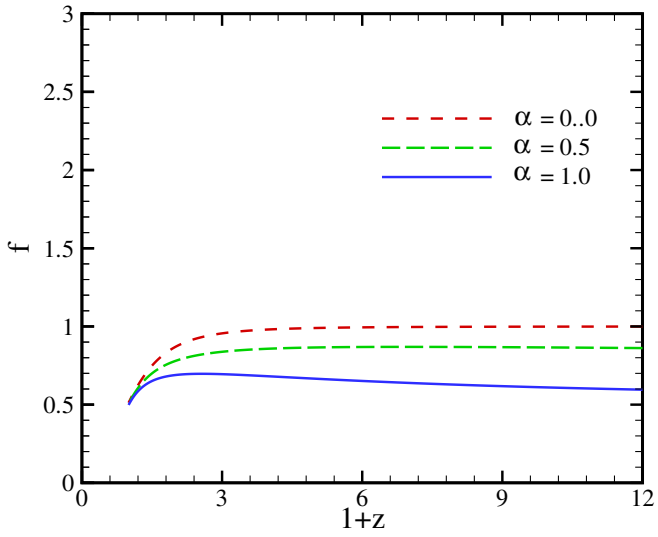

FIG. 14 (color online). Growth index versus redshift for different values of α. Here we took a typical values for the cosmological parameters as $\Omega_m = 0.3$ and $\Omega_{\rm tot} = 1.0$ and $w_0 = -1.0$.

ter of $\beta = f/b = 0.49 \pm 0.09$ at $z = 0.15$, where b is the bias parameter, describes the difference in the distribution of galaxies and mass. Verde *et al.* (2003) used the bispectrum of 2dFGRS galaxies [46,47] and obtained $b_{\rm verde} = 1.04 \pm 0.11$ which resulted $f = 0.51 \pm 0.10$. Now we fit the growth index at the present time derived from the Eq. (33) with the observational value. This fitting gives a loss constraint to the parameters of the model, so in order to have a better confinement of the parameters, we combine this fitting with those of SNIa + CMB + SDSS which has been discussed in the last section. We perform the least square fitting by minimizing $\chi^2 = \chi^2_{\rm SNIa} + \chi^2_{\rm CMB} + \chi^2_{\rm SDSS} + \chi^2_{\rm LSS}$. The best fit values with the corresponding error bars for the model parameters are: $\Omega_m = 0.31^{+0.02}_{-0.04}$, $\alpha = 0.80^{+0.70}_{-0.30}$ and $w_0 = -1.40^{+0.40}_{-0.65}$ at 1σ confidence level with $\chi^2_{\rm min}/N_{\rm d.o.f} = 1.15$. The error bars have been obtain through the likelihood functions ($\mathcal{L} \propto e^{-\chi^2/2}$) marginalizing over the nuisance parameter of h [48]. The

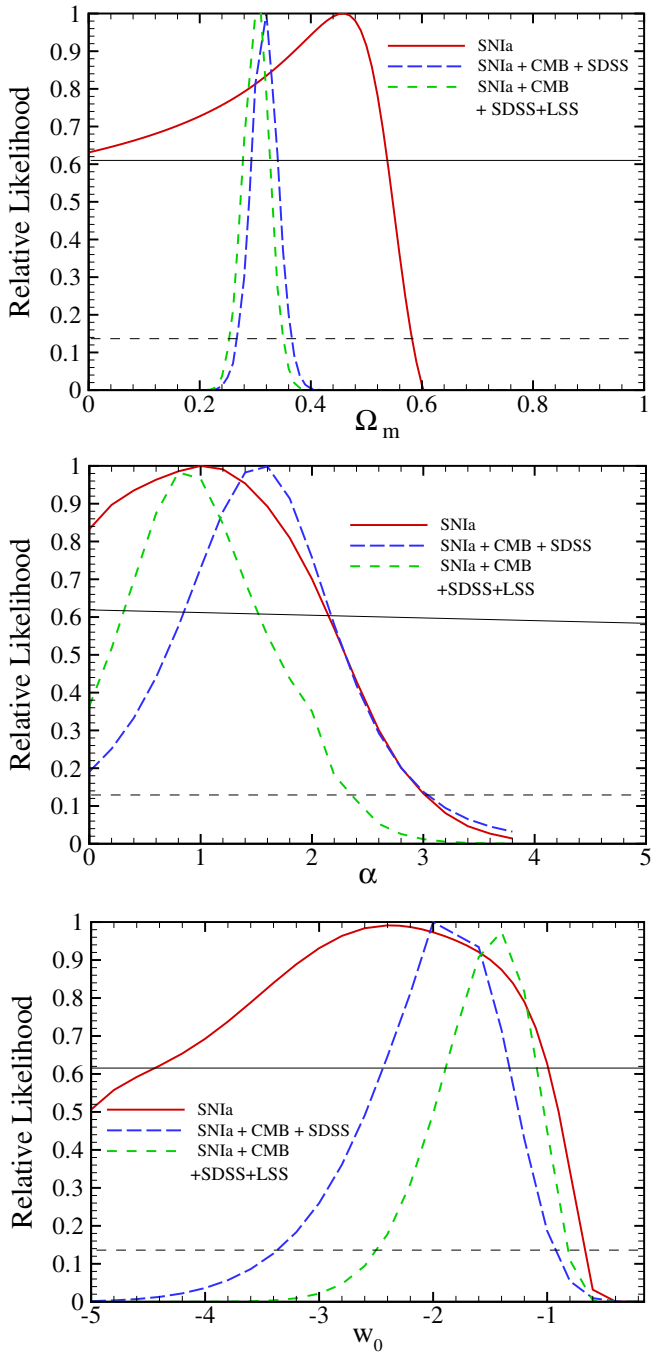

FIG. 15 (color online). Marginalized likelihood functions of three parameters of dark energy model (Ω_m, α and w_0). The solid line corresponds to the likelihood function of fitting the model with SNIa data, the long dashed line with the joint SNIa + CMB + SDSS data and dashed line corresponds to SNIa + CMB + SDSS + LSS. The intersections of the curves with the horizontal solid and dashed lines give the bounds with 1σ and 2σ level of confidence, respectively.

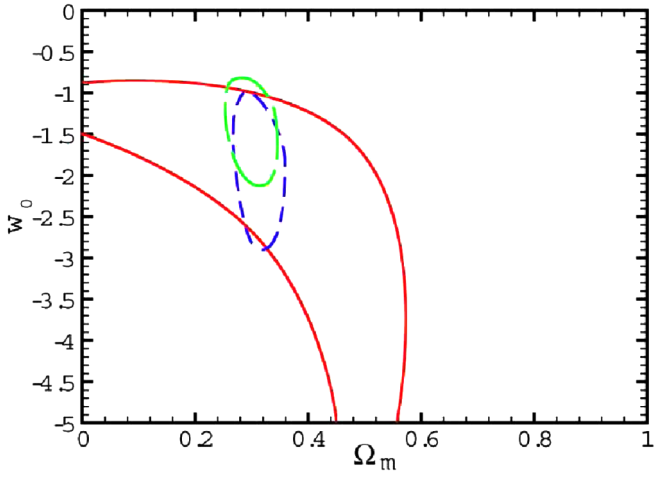

FIG. 16 (color online). Joint confidence intervals of Ω_m and w_0, fitting with SNIa (solid line), SNIa + CMB + SDSS (dashed line) and SNIa + CMB + SDSS + LSS (long dashed line) with 1σ level of confidence.

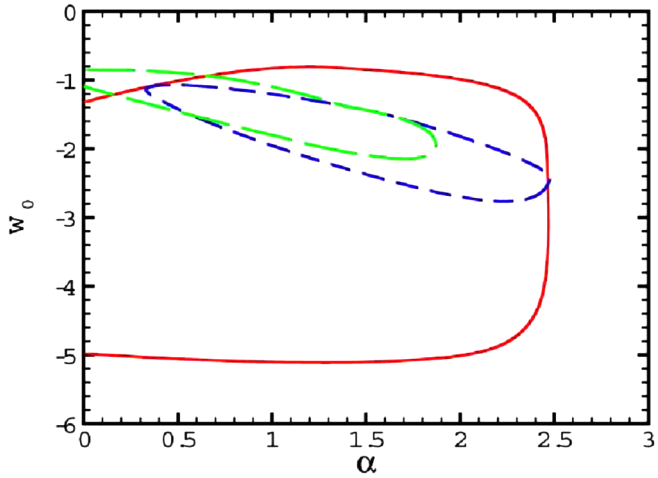

FIG. 17 (color online). Joint confidence intervals of α and w_0, fitting with the SNIa (solid line), SNIa + CMB + SDSS (dashed line) and SNIa + CMB + SDSS + LSS (long dashed line) with 1σ level of confidence.

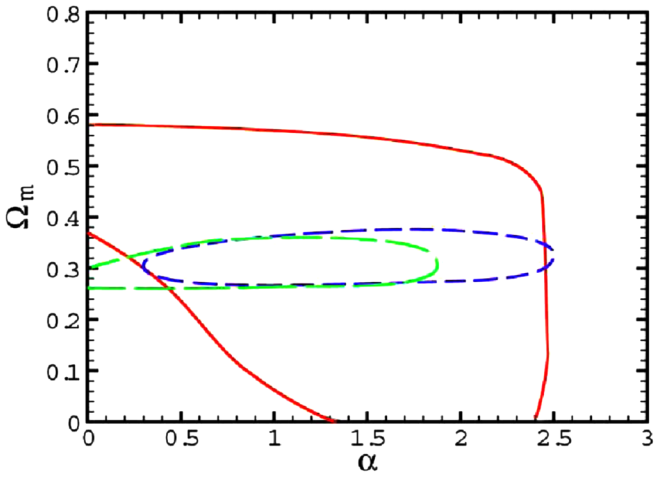

FIG. 18 (color online). Joint confidence intervals of Ω_m and α, fitting with the SNIa (solid line), SNIa + CMB + SDSS (dashed line) and SNIa + CMB + SDSS + LSS (long dashed line) with 1σ level of confidence.

Hubble parameter corresponds to the minimum value of χ^2 is $h = 0.65$. The likelihood functions for the three cases of (i) fitting model with Supernova data, (ii) combined analysis with the three experiments of SNIa + CMB + SDSS and (iii) combining all four experiments of SNIa + CMB + SDSS + LSS are shown in Fig. 15. The joint confidence contours in the (Ω_m, w_0), (α, Ω_m) and (w_0, α) planes also are shown in Figs. 16–18.

Finally we do the consistency test, comparing the age of universe derived from this model with the age of old stars and Old High Redshift Galaxies (OHRG) in various redshifts. Table II shows that the age of universe from the combined analysis of SNIa + CMB + SDSS + LSS is 13.72 Gyr which is in agreement with the age of old stars [28]. Here we take three OHRG for comparison with the power-law dark energy model, namely, the LBDS 53W091, a 3.5-Gyr old radio galaxy at $z = 1.55$ [49], the LBDS 53W069 a 4.0-Gyr old radio galaxy at $z = 1.43$ [50] and a quasar, APM 08279 + 5255 at $z = 3.91$ with an age of $t = 2.1^{+0.9}_{-0.1}$ Gyr [51]. The later one has once again led to the "age crisis". An interesting point about this quasar is that it cannot be accommodated in the ΛCDM model [52]. To quantify the age-consistency test we introduce the expression τ as:

$$\tau = \frac{t(z; \alpha, w_0, \Omega_m)}{t_{\rm obs}} = \frac{t(z; \alpha, w_0, \Omega_m) H_0}{t_{\rm obs} H_0}, \qquad (34)$$

where $t(z)$ is the age of universe from the Eq. (18) and $t_{\rm obs}$ is an estimation for the age of old cosmological object. $\tau >$ 1 provides a compatible age for the universe. Table III shows the value of τ for three mentioned OHRG. We see that the parameters of dark energy model from the SNIa and CMB observations do not provide a compatible age for the universe, however combining with the LSS data results a longer age for the universe. Once again in the power-law dark energy model, APM 08279 + 5255 at $z = 3.91$ has longer age than the universe.

TABLE III. The value of τ for three high redshift objects, using the parameters of the model derived from the fitting with the observations.

Observation	LBDS 53W069	LBDS 53W091	APM 08279 + 5255
	$z = 1.43$	$z = 1.55$	$z = 3.91$
SNIa	0.92	0.97	0.59
SNIa + CMB + SDSS	0.83	0.88	0.50
SNIa + CMB + SDSS + LSS	1.01	1.07	0.65

VI. CONCLUSION

We proposed a power-law parametrized dark energy model with the mean-equation of state of $\bar{w}(z) = w_0 a^\alpha$. An equivalent quintessence potential of scalar field was calculated for this model. The effect of this model on the age of universe, radial comoving distance, comoving volume element and the variation of apparent size of objects with the redshift (Alcock-Paczynski test) have been studied. In order to constrain the parameters of model we fit our model with the Gold sample SNIa data, CMB shift parameter, location of baryonic acoustic peak observed by SDSS and large scale structure data by 2dFGRS. The best parameters from the fitting obtained as: $h = 0.65$, $\Omega_m = 0.31^{+0.02}_{-0.04}$, $\alpha = 0.80^{+0.70}_{-0.30}$ and $w_0 = -1.40^{+0.40}_{-0.65}$ at 1σ confidence level with $\chi^2_{\rm min}/N_{\rm d.o.f} = 1.15$, theoretical attempts for $w < -1$ can be found in [53–58].

We also did the age test, comparing the age of old stars and old high redshift galaxies with the age derived from the power-law dark energy model. From the best fit parameters of the model we obtained an age of 13.72 Gyr for the universe which is in agreement with the age of old stars. We also chose two high redshift radio galaxies at $z = 1.55$ and $z = 1.43$ with a quasar at $z = 3.91$. The two first objects were consistent with the age of universe by means that there were younger than the age of universe while the later one was older than the age of universe.

[1] A. G. Riess *et al.*, Astron. J. **116**, 1009 (1998).
[2] S. Perlmutter *et al.*, Astrophys. J. **517**, 565 (1999).
[3] C. L. Bennett *et al.*, Astrophys. J. Suppl. Ser. **148**, 1 (2003).

[4] H. V. Peiris *et al.*, Astrophys. J. Suppl. Ser. **148**, 213 (2003).
[5] D. N. Spergel, L. Verde, H. V. Peiris *et al.*, Astrophys. J. **148**, 175 (2003).
[6] S. Weinberg, Rev. Mod. Phys. **61**, 1 (1989); S. M. Carroll, Living Rev. Relativity **4**, 1 (2001); P. J. E. Peebles and B. Ratra, Rev. Mod. Phys. **75**, 559 (2003); T. Padmanabhan, Phys. Rep. **380**, 235 (2003).
[7] C. Wetterich, Nucl. Phys. **B302**, 668 (1988); P. J. E. Peebles and B. Ratra, Astrophys. J. **325**, L17 (1988); B. Ratra and P. J. E. Peebles, Phys. Rev. D **37**, 3406 (1988); J. A. Frieman, C. T. Hill, A. Stebbins, and I. Waga, Phys. Rev. Lett. **75**, 2077 (1995); M. S. Turner and M. White, Phys. Rev. D **56**, R4439 (1997); R. R. Caldwell, R. Dave, and P. J. Steinhardt, Phys. Rev. Lett. **80**, 1582 (1998); A. R. Liddle and R. J. Scherrer, Phys. Rev. D **59**, 023509 (1999); I. Zlatev, L. Wang, and P. J. Steinhardt, Phys. Rev. Lett. **82**, 896 (1999); P. J. Steinhardt, L. Wang, and I. Zlatev, Phys. Rev. D **59**, 123504 (1999); D. F. Torres, Phys. Rev. D **66**, 043522 (2002).
[8] L. Amendola, Phys. Rev. D **62**, 043511 (2000); L. Amendola and D. Tocchini-Valentini, Phys. Rev. D **64**, 043509 (2001); **66**, 043528 (2002); L. Amendola, Mon. Not. R. Astron. Soc. **342**, 221 (2003); M. Pietroni, Phys. Rev. D **67**, 103523 (2003); D. Comelli, M. Pietroni, and A. Riotto, Phys. Lett. B **571**, 115 (2003); U. Franca and R. Rosenfeld, Phys. Rev. D **69**, 063517 (2004); X. Zhang, Mod. Phys. Lett. A **20**, 2575 (2005); Phys. Lett. B **611**, 1 (2005).
[9] P. J. E. Peebles and R. Ratra, Astrophys. J. **325**, L17 (1988).
[10] C. Armendariz-Picon, V. Mukhanov, and P. J. Steinhardt, Phys. Rev. Lett. **85**, 4438 (2000).
[11] J. S. Bagla, H. K. Jassal, and T. Padmanabhan, Phys. Rev. D **67**, 063504 (2003).
[12] R. R. Caldwell, Phys. Lett. B **545**, 23 (2002).
[13] R. R. Caldwell, M. Kamionkowski, and N. N. Weinberg, Phys. Rev. Lett. **91**, 071301 (2003).
[14] A. Kamenshchik, U. Moschella, and V. Pasquier, Phys. Lett. B **511**, 265 (2001).
[15] S. Arbabi Bidgoli, M. S. Movahed, and S. Rahvar, Int. J. Mod. Phys. D **15**, 1455 (2006).
[16] M. Sadegh Movahed and Sohrab Rahvar, Phys. Rev. D **73**, 083518 (2006).
[17] L. Wang, R. R. Caldwell, J. P. Ostriker, and P. J. Steinhardt, Astrophys. J. **530**, 17 (2000).
[18] S. Perlmutter, M. S. Turner, and M. White, Phys. Rev. Lett. **83**, 670 (1999).
[19] L. Page *et al.*, Astrophys. J. Suppl. Ser. **148**, 233 (2003).
[20] M. Doran, M. Lilley, J. Schwindt, and C. Wetterich, Astrophys. J. **559**, 501 (2001).
[21] M. Doran and M. Lilley, Mon. Not. R. Astron. Soc. **330**, 965 (2002).
[22] R. R. Caldwell and M. Doran, Phys. Rev. D **69**, 103517 (2004).
[23] M. Chevallier, D. Polarski, and A. Starobinsky, Int. J. Mod. Phys. D **10**, 213 (2001).
[24] E. V. Linder, Phys. Rev. Lett. **90**, 091301 (2003).
[25] U. Seljak *et al.*, Phys. Rev. D **71**, 103515 (2005).
[26] C. Alcock and B. Paczynski, Nature (London) **281**, 358 (1979).
[27] A. G. Riess *et al.*, Astrophys. J. **607**, 665 (2004).
[28] E. Carretta *et al.*, Astrophys. J. **533**, 215 (2000); L. M. Krauss and B. Chaboyer, astro-ph/0111597; B. Chaboyer and L. M. Krauss, Astrophys. J. Lett. **567**, L45 (2002).
[29] H. B. Richer *et al.*, Astrophys. J. **574**, L151 (2002).
[30] B. M. S. Hansen *et al.*, Astrophys. J. **574**, L155 (2002).
[31] B. P. Schmidt *et al.*, Astrophys. J. **507**, 46 (1998).
[32] J. L. Tonry *et al.*, Astrophys. J. **594**, 1 (2003).
[33] B. J. Barris *et al.*, Astrophys. J. **602**, 571 (2004).
[34] A. Melchiorri, L. Mersini, C. L. Ödman, and M. Trodden, Phys. Rev. D **68**, 043509 (2003).
[35] W. L. Freedman *et al.*, Astrophys. J. Lett. **553**, 47 (2001).
[36] X. Zhang and F. Q. Wu, Phys. Rev. D **72**, 043524 (2005).
[37] C. L. Bennett, R. S, Hill, and G. Hinshaw, Astrophys. J. Suppl. Ser. **148**, 97 (2003).
[38] W. Hu and N. Sugiyama, Astrophys. J. **444**, 489 (1995).
[39] J. R. Bond, G. Efstathiou, and M. Tegmark, Mon. Not. R. Astron. Soc. **291**, L33 (1997); A. Melchiorri, L. Mersini, C. J. Odman, and M. Trodden, Phys. Rev. D **68**, 043509 (2003); C. J. Odman, A. Melchiorri, M. P. Hobson, and A. N. Lasenby, Phys. Rev. D **67**, 083511 (2003).
[40] T. J. Pearson *et al.* (CBI Collaboration), Astrophys. J. **591**, 556 (2003); C. L. Kuo *et al.* (ACBAR Collaboration), Astrophys. J. **600**, 32 (2004).
[41] D. J. Eisenstein *et al.*, Astrophys. J. **633**, 560 (2005).
[42] T. Padmanabhan, *Structure Formation in the Universe* (Cambridge Univ. Press, Cambridge, England, 1993).
[43] R. H. Brandenberger, in *The Early Universe and Observational Cosmology*, edited by N. Breton, J. L. Cervantes-Cota, and M. Salgado, Lecture Notes in Physics, Vol. 646 (Springer, Berlin Heidelberg, 2004), p. 127.
[44] P. J. E. Peebles, *The Large Scale Structure of the Universe* (Princeton University Press, Princeton, NJ, 1980).
[45] R. Mansouri and S. Rahvar, Int. J. Mod. Phys. D **11**, 312 (2002).
[46] L. Verde, M. Kamionkowski, J. J. Mohr, and A. J. Benson, Mon. Not. R. Astron. Soc. **321**, L7 (2001).
[47] O. Lahav, S. L. Bridle, and W. J. Percival (2dFGRS Team), Mon. Not. R. Astron. Soc. **333**, 961 (2002).
[48] W. H. Press, S. A. Teukolsky, W. T. Vettering, and B. P. Flannery, *Numerical Recipes* (Cambridge University Press, Cambridge, 1994).
[49] J. Dunlop *et al.*, Nature (London) **381**, 581 (1996); H. Spinrard, Astrophys. J. **484**, 581 (1997).
[50] J. Dunlop, in *The Most Distant Radio Galaxies*, edited by H. J. A. Rottgering, P. Best, and M. D. Lehnert (Kluwer, Dordrecht, 1999), p. 71.
[51] G. Hasinger, N. Schartel, and S. Komossa, Astrophys. J. Lett. **573**, L77 (2002); S. Komossa and G. Hasinger, astro-ph/0207321.
[52] D. Jain and A. Dev, Phys. Lett. B **633**, 436 (2006).
[53] R. R. Caldwell, Phys. Lett. B **545**, 23 (2002).
[54] A. E. Schulz and M. J. White, Phys. Rev. D **64**, 043514 (2001).
[55] L. Parker and A. Raval, Phys. Rev. D **60**, 063512 (1999).
[56] P. H. Frampton, Phys. Lett. B **555**, 139 (2003).
[57] M. Ahmed, S. Dodelson, P. B. Greene, and R. Sorkin, Phys. Rev. D **69**, 103523 (2004).
[58] S. M. Carroll, M. Hoffman, and M. Trodden, Phys. Rev. D **68**, 023509 (2003).